Comput Visual Sci (2008) 11:67–76
DOI 10.1007/s00791-007-0061-1

REGULAR ARTICLE

A stabilized difference scheme for deformable porous media and its numerical resolution by multigrid methods

F. J. Gaspar · F. J. Lisbona · C. W. Oosterlee

Received: 15 January 2006 / Accepted: 24 May 2006 / Published online: 8 February 2007

Abstract This paper deals with the 2D system of incompressible poroelasticity equations in which an artificial stabilization term has been added to the discretization on collocated grids. Two issues are discussed: It is proved and shown that the additional term indeed brings stability and does not spoil the second order accurate convergence. Secondly, various smoothers are examined in order to find an optimal multigrid method for the discrete system of equations. Numerical experiments confirm the stability and the second order accuracy, as well as fast multigrid convergence for a realistic poroelasticity experiment.

Communicated by P. Wesseling.

This research has been partially supported by the INTAS project 03-50-4395, the Spanish project MEC/FEDER MTM 2004-019051, the Diputación General de Aragón and the Dutch program BSIK: knowledge and research capacity, in the ICT project BRICKS (http://www.bsik-bricks.nl), theme MSV1.

F. J. Gaspar (✉)
Departamento de Matemática Aplicada,
University of Zaragoza, Maria de Luna 3,
50018 Zaragoza, Spain
e-mail: fjgaspar@unizar.es

F. J. Lisbona
Departamento de Matemática Aplicada,
University of Zaragoza, Pedro Cerbuna 12,
50009 Zaragoza, Spain
e-mail: lisbona@unizar.es

C. W. Oosterlee
Delft Institute of Applied Mathematics,
Delft University of Technology, Mekelweg 4,
2628 Delft, The Netherlands
e-mail: c.w.oosterlee@math.tudelft.nl

1 Introduction

The classical quasi-static Biot model [1–3] for soil consolidation, mathematically describes the time dependent interaction between the deformation of an elastic porous material and the fluid flow inside of it. This model can be formulated as a system of partial differential equations for the unknowns displacement and pressure. By $\mathbf{u} = (u, v)$ we denote the displacement vector and by p the pore pressure of the fluid. Here, we consider the case of a homogeneous, isotropic and incompressible medium Ω, so the governing equations are given by

$$-\mu\tilde{\Delta}\mathbf{u} - (\lambda+\mu)\text{grad}\,\text{div}\,\mathbf{u} + \text{grad}\,p = \mathbf{g}(\mathbf{x},t), \tag{1}$$

$$\frac{\partial}{\partial t}(\text{div}\,\mathbf{u}) - \frac{\kappa}{\eta}\Delta p = f(\mathbf{x},t), \quad \mathbf{x}\in\Omega,\ 0<t\le T, \tag{2}$$

where λ and μ are the Lamé coefficients, κ is the permeability of the porous medium, η is the viscosity of the fluid and $\tilde{\Delta}$ represents the vector Laplace operator. The quantity $\text{div}\,\mathbf{u}\,(\mathbf{x},t)$ is the dilatation, i.e. the volume increase rate of the system, which can be considered as a measure of the change in porosity of the soil. The source terms $\mathbf{g}(\mathbf{x},t)$ and $f(\mathbf{x},t)$ are supposed to be in $(L^2(\Omega))^2$ and $L^2(\Omega)$, respectively. They are used to represent a density of applied body forces and a forced fluid extraction or injection process for each case.

For simplicity in the analysis of the convergence of the schemes, we assume here that $\partial\,\Omega$ is rigid (zero displacements) and permeable (free drainage), so that we have homogeneous Dirichlet boundary conditions,

$$\mathbf{u}(\mathbf{x},t) = 0, \quad p(\mathbf{x},t) = 0, \quad \mathbf{x}\in\partial\,\Omega. \tag{3}$$

Other more realistic boundary conditions (such as natural boundary conditions) can be studied in the same framework. For completeness, we will consider in last section an example including a traction on the boundary.

Before fluid starts to flow and due to the incompressibility of the solid and fluid phases, the initial state satisfies

$$\operatorname{div}\mathbf{u}(\mathbf{x},0)=0,\quad \mathbf{x}\in\Omega. \tag{4}$$

When a load is applied on an elastic saturated porous medium, the pressure suddenly increases and a sharp boundary layer appears in the early stages of the time-dependent process. In the case of an unstable discretization, unphysical oscillations appear in the first time steps of the numerical solution. After this phase, the solution shows a much smoother behaviour and these oscillations tend to disappear. Some care is needed in the construction of stable discretizations for the whole process. Whereas a significant development has taken place in the finite element treatment of this problem (see, for example [8,10],), we aim at the development of stable and accurate finite difference schemes for incompressible poroelasticity on Cartesian grids. This is done having in mind rectangular domains for consolidation problems, as well as the availability of highly efficient iterative multigrid solution techniques for the resulting discrete problems.

A staggered grid discretization approach has been presented in [4,5]. Pressure points in the staggered grid were located at the vertices of the cells while the displacement points were defined at the cell faces. This approach guaranteed stable schemes, independently of discretization parameters, that are second order convergent in discrete energy norms. An efficient multigrid solver for the system of poroelasticity equations discretized on the staggered grid has been developed in [6,13]. However, the choice for a staggered grid is a rigorous one. Staggered grid discretizations may not be easily generalized to curved domains, or to unstructured grids.

The discretization by standard central finite differences of a *transformed problem on a collocated grid* [7] does not produce unphysical oscillations. More precisely, with the introduction of new variables $q=-\Delta p$ and $\mathbf{v}=\frac{\partial\mathbf{u}}{\partial t}$, an equivalent transformed system reads

$$-\mu\tilde{\Delta}\mathbf{v}+\operatorname{grad}\left(\frac{\partial p}{\partial t}+(\lambda+\mu)\,\frac{\kappa}{\eta}q\right)=(\lambda+\mu)\operatorname{grad}f+\frac{\partial\mathbf{g}}{\partial t},$$
$$q+\Delta p=0,$$

$$\frac{\partial q}{\partial t}-(\lambda+2\mu)\frac{\kappa}{\eta}\Delta q=-(\lambda+2\mu)\Delta f-\operatorname{div}\frac{\partial\mathbf{g}}{\partial t}, \tag{5}$$

with $\mathbf{v}=\mathbf{0}$, $p=0$, $\operatorname{div}\mathbf{v}+\frac{\kappa}{\eta}q=f$ as the boundary conditions. Moreover, for a 1D discrete poroelasticity model the corresponding numerical scheme appears to be equivalent to a discretization by central differences on a collocated grid of a poroelasticity equation *with a perturbation term* $\varepsilon\frac{\partial\Delta p}{\partial t}$, with $\varepsilon=\frac{h^2}{4(\lambda+2\mu)}$.
The new problem reads

$$-\mu\tilde{\Delta}\mathbf{u}-(\lambda+\mu)\operatorname{grad}\operatorname{div}\mathbf{u}+\operatorname{grad}p=\mathbf{g}(\mathbf{x},t), \tag{6}$$
$$\frac{\partial}{\partial t}(\operatorname{div}\mathbf{u}-\varepsilon\Delta p)-\frac{\kappa}{\eta}\Delta p=f(\mathbf{x},t), \tag{7}$$

which needs be supplied by the initial condition

$$\operatorname{div}\mathbf{u}(\mathbf{x},0)-\varepsilon\,\Delta p(\mathbf{x},0)=0.$$

In addition to favorable stability, excellent convergence for the decoupled treatment of system (5) was obtained by employing scalar multigrid methods for each of the equations in (5) separately [7]. However, the system transformation may not be easily performed in the case of heterogeneous media, in which coefficients are not constant. Furthermore, the straightforward decoupled treatment of (5) gave only $\mathcal{O}(\tau)$ accuracy in time, with τ the time step, as the unknowns in the boundary conditions are lagging one time step behind.

In this paper we generalize the benefits of the approach in [7] to two-dimensional problems, however, by explicitly adding an artificial pressure term to Eq. (2). So, we work on a collocated grid, with the original equations in which a stabilization term is added. In Sect. 3 we present the 2D stability and convergence properties of the discretization.

When discretizing the incompressible poroelasticity equations with standard second order discretizations and an artificial pressure term, the development of multigrid smoothing methods is not straightforward. Smoothing factors of standard collective point-wise relaxations are not satisfactory. A possibility to overcome this problem is to extend the idea of box relaxation, which has proved to be a suitable smoother in the case of staggered grid discretizations, to the non-staggered case (for incompressible Navier–Stokes equations, for example, in [9]). The development of such smoothers is pursued in Sect. 4. As in the staggered case, box relaxation should be replaced by a corresponding box-line version, if significant anisotropies occur.

In Sect. 5 different smoothers are compared in the multigrid solution of reference experiments.

2 A stabilized difference scheme

In the construction of difference schemes for the solution of problem (6) and (7) we begin by the space approximation. For simplicity in notation, we consider the problem on the unit square and introduce a uniform grid with the same mesh size in each direction. Let ω be the set of internal nodes of the grid

$$\omega = \{(ih,\, jh)\,,\; i,j = 1,\ldots,N-1\}$$

where $h = 1/N$, with $N \in \mathbb{N}$ and $\partial\omega$ the set of boundary nodes. The finite difference solution of (1) – (4) will be denoted by $\mathbf{u}_h(\mathbf{x},t), p_h(\mathbf{x},t)\,, \mathbf{x} \in \omega \cup \partial\omega,\; 0 < t \le T$. Using the standard index-free notation of the theory of difference schemes [11], for the right, left and central difference derivatives we write

$$w_x = \frac{w(x+h)-w(x)}{h}, \quad w_{\bar{x}} = \frac{w(x)-w(x-h)}{h},$$
$$w_{\overset{\circ}{x}} = \frac{w(x+h)-w(x-h)}{2h}.$$

The second difference derivative is given by

$$w_{\bar{x}x} = \frac{1}{h}(w_x - w_{\bar{x}}) = \frac{w(x+h)-2w(x)+w(x-h)}{h^2}.$$

For grid functions vanishing on $\partial\omega$, we consider the Hilbert space $H = L_2(\omega)$, with scalar product and norm given by

$$(y,w) = \sum_{x\in\omega} ywh^2, \quad \|y\| = (y,y)^{1/2}.$$

Let us introduce $\widetilde{H} = H \oplus H$, for vector-valued functions that are zero on $\partial\omega$, with

$$(\mathbf{y},\mathbf{w}) = (y_1,w_1) + (y_2,w_2), \quad \|\mathbf{y}\| = (\mathbf{y},\mathbf{y})^{1/2}.$$

Given a selfadjoint and positive definite operator C, H_C denotes the space H, supplied by the scalar product $(y,w)_C = (Cy,w)$ and norm $\|y\|_C = (Cy,y)^{1/2}$. We approximate the differential operator of the elasticity part $-\mu\tilde{\Delta} - (\lambda+\mu)$grad div by the difference operator

$$A = \begin{pmatrix} A_{11} & A_{12} \\ A_{21} & A_{22} \end{pmatrix},$$
$$A_{11}y = -\mu\Delta_h y - (\lambda+\mu)\, y_{\bar{x}_1x_1}, \tag{8}$$
$$A_{12}y = A_{21}y = -\frac{\lambda+\mu}{2}(y_{\bar{x}_1x_2} + y_{x_1\bar{x}_2}),$$
$$A_{22}y = -\mu\Delta_h y - (\lambda+\mu)\, y_{\bar{x}_2x_2},$$

where the usual five-point stencil approximation of the Laplace operator is used: $\Delta_h y = y_{\bar{x}_1x_1} + y_{\bar{x}_2x_2}$. For $\mathbf{y},\mathbf{w} \in \widetilde{H}$ we have $(A\mathbf{y},\mathbf{w}) = (\mathbf{y},A\mathbf{w})$. In addition to that we have $-\mu\tilde{\Delta}_h \le A \le -(\lambda+2\mu)\tilde{\Delta}_h$, with $\tilde{\Delta}_h = \begin{pmatrix} \Delta_h & 0 \\ 0 & \Delta_h \end{pmatrix}$. Due to $A = A^* \ge \mu\delta_h\widetilde{E}$, with $\delta_h > 0$ being the minimum eigenvalue of operator Δ_h and $\widetilde{E}$ the identity operator in $\widetilde{H}$, the difference operator A is selfadjoint and positive definite. To approximate the diffusion operator Δ, we shall use $By = -\Delta_h y$, so that $B = B^* \ge \delta_h E$ with E the identity operator in H. To approximate the coupling terms, grad p and div $\mathbf{u}$, we use second order approximations

$$Gy = (y_{\overset{\circ}{x}_1}, y_{\overset{\circ}{x}_2}), \quad \text{for } y \in H,$$
$$D\mathbf{w} = (w_1)_{\overset{\circ}{x}_1} + (w_2)_{\overset{\circ}{x}_2}, \quad \text{for } \mathbf{w} \in \widetilde{H}.$$

Operators $G : H \to \widetilde{H}$ and $D : \widetilde{H} \to H$ verify the property $(Gp_h, \mathbf{u}_h) = -(p_h, D\mathbf{u}_h)$.

After the spatial approximation of (6–7) we arrive at a Cauchy problem for the system of differential-difference equations

$$A\mathbf{u}_h + Gp_h = \mathbf{g_h}(\mathbf{x},t), \tag{9}$$
$$\frac{d}{dt}\left(D\mathbf{u}_h + \frac{h^2}{4(\lambda+2\mu)}Bp_h\right) + \frac{\kappa}{\eta}Bp_h = f_h(\mathbf{x},t), \tag{10}$$

with the initial condition $D\mathbf{u}_h(0) + \frac{h^2}{4(\lambda+2\mu)}Bp_h(0) = 0$. We now construct a simple difference scheme in time for the approximation of the solution $\{\mathbf{u}_h\,, p_h\}$ of the Cauchy problem. We use a uniform grid for time discretization with step-size $\tau > 0$. Let $y^m(\mathbf{x}) = y(\mathbf{x},t_m)$, where $t_m = m\tau,\; m = 0,1,\ldots,M,\; M\tau = T$. The implicit Euler scheme then reads

$$A\mathbf{u}_h^{m+1} + Gp_h^{m+1} = \mathbf{g}_h^{m+1}, \tag{11}$$
$$\frac{D\mathbf{u}_h^{m+1} - D\mathbf{u}_h^m}{\tau} + \frac{h^2}{4(\lambda+2\mu)}\frac{Bp_h^{m+1} - Bp_h^m}{\tau}$$
$$+\frac{\kappa}{\eta}Bp_h^{m+1} = f_h^{m+1}, \tag{12}$$

where the initial condition has already been incorporated. Other discretizations can easily be obtained if, for example, two-level weighted schemes are used for time stepping. The second order accurate Crank–Nicolson scheme is applied in the numerical experiments in Sect. 5.

3 Convergence of the stabilized scheme

We give an energy estimate for the stabilized discrete problem (11)–(12). For simplicity, suppose that p_h^0 satisfies the boundary conditions. Otherwise, a different estimate must be used for the first time step (see [5]).

Proposition 1 *The solutions of scheme* (11)–(12) *for* $m \geq 0$ *satisfy the a priori estimates*

$$\|\mathbf{u}_h^{m+1}\|_A^2 \leq 2\|\mathbf{u}_h^0\|_A^2 + \frac{h^2}{2(\lambda+2\mu)}\|p_h^0\|_B^2 + 2\|\mathbf{g}_h^{m+1}\|_{A^{-1}}^2 + C_1\left(\tau\sum_{j=1}^{m+1}\|f_h^j\|_{B^{-1}}^2 + \tau\sum_{j=0}^{m}\|\frac{\mathbf{g}_h^{j+1}-\mathbf{g}_h^j}{\tau}\|_{A^{-1}}^2\right), \tag{13}$$

$$\|p_h^{m+1}\|_B^2 \leq 2\|p_h^0\|_B^2 + C_2\left(\tau\sum_{j=0}^{m}\|\frac{f_h^{j+1}-f_h^j}{\tau}\|_{B^{-1}}^2 + \tau\sum_{j=0}^{m}\|\frac{\mathbf{g}_h^{j+1}-\mathbf{g}_h^j}{\tau}\|_{A^{-1}}^2 + \|f_h^{m+1}\|_{B^{-1}}^2\right), \tag{14}$$

where C_1 *and* C_2 *are constants independent of the discretization parameters.*

Proof To obtain an a priori estimate for the displacements, solution $\mathbf{u}_h^{m+1}$ is splitted up into two parts, $\mathbf{u}_h^{m+1} = \overline{\mathbf{u}}_h^{m+1} + \overline{\overline{\mathbf{u}}}_h^{m+1}$. The first part $\overline{\mathbf{u}}_h^{m+1}$, is the solution of the problem

$$A\overline{\mathbf{u}}_h^{m+1} = \mathbf{g}_h^{m+1}, \tag{15}$$

and the second part $\overline{\overline{\mathbf{u}}}_h^{m+1}$ is the solution of

$$A\overline{\overline{\mathbf{u}}}_h^{m+1} + Gp_h^{m+1} = 0, \tag{16}$$

$$\frac{D\overline{\overline{\mathbf{u}}}_h^{m+1} - D\overline{\overline{\mathbf{u}}}_h^{m}}{\tau} + \frac{h^2}{4(\lambda+2\mu)}\frac{Bp_h^{m+1}-Bp_h^m}{\tau} + \frac{\kappa}{\eta}Bp_h^{m+1} = f_h^{m+1} - \frac{D\overline{\mathbf{u}}_h^{m+1} - D\overline{\mathbf{u}}_h^m}{\tau}. \tag{17}$$

After multiplying scalarly (16) and (17) by $(\overline{\overline{\mathbf{u}}}_h^{m+1} - \overline{\overline{\mathbf{u}}}_h^m)/\tau$ and p_h^{m+1}, respectively, we get for $0 \leq m \leq M-1$,

$$\left(A\overline{\overline{\mathbf{u}}}_h^{m+1}, \frac{\overline{\overline{\mathbf{u}}}_h^{m+1}-\overline{\overline{\mathbf{u}}}_h^m}{\tau}\right) + \left(Gp_h^{m+1}, \frac{\overline{\overline{\mathbf{u}}}_h^{m+1}-\overline{\overline{\mathbf{u}}}_h^m}{\tau}\right) = 0, \tag{18}$$

and

$$\left(D\frac{\overline{\overline{\mathbf{u}}}_h^{m+1}-\overline{\overline{\mathbf{u}}}_h^m}{\tau}, p_h^{m+1}\right) + \frac{\kappa}{\eta}\left(Bp_h^{m+1}, p_h^{m+1}\right) + \frac{h^2}{4(\lambda+2\mu)}\left(B\frac{p_h^{m+1}-p_h^m}{\tau}, p_h^{m+1}\right) = \left(f_h^{m+1}, p_h^{m+1}\right) - \left(\frac{D\overline{\mathbf{u}}_h^{m+1} - D\overline{\mathbf{u}}_h^m}{\tau}, p_h^{m+1}\right). \tag{19}$$

The addition of (18) and (19) yields

$$\left(A\overline{\overline{\mathbf{u}}}_h^{m+1}, \overline{\overline{\mathbf{u}}}_h^{m+1} - \overline{\overline{\mathbf{u}}}_h^m\right) + \tau\frac{\kappa}{\eta}B\left(p_h^{m+1}, p_h^{m+1}\right) + \frac{h^2}{4(\lambda+2\mu)}\left(B(p_h^{m+1}-p_h^m), p_h^{m+1}\right) = \tau\left(f_h^{m+1}, p_h^{m+1}\right) - \left(D\overline{\mathbf{u}}_h^{m+1} - D\overline{\mathbf{u}}_h^m, p_h^{m+1}\right). \tag{20}$$

Applying the generalized Cauchy–Schwarz inequality at the right-hand side, we get

$$\frac{1}{2}\left(\|\overline{\overline{\mathbf{u}}}_h^{m+1}\|_A^2 - \|\overline{\overline{\mathbf{u}}}_h^m\|_A^2\right) + \frac{h^2\left(\|p_h^{m+1}\|_B^2 - \|p_h^m\|_B^2\right)}{8(\lambda+2\mu)} \leq \frac{\tau\eta}{2\kappa}\|f_h^{m+1}\|_{B^{-1}}^2 + \frac{\tau\eta}{2\kappa}\|D\frac{\overline{\mathbf{u}}_h^{m+1}-\overline{\mathbf{u}}_h^m}{\tau}\|_{B^{-1}}^2, \tag{21}$$

and therefore (13) is obtained, i.e., the solution $\mathbf{u}_h$ is stable with respect to the initial data and right-hand side.

To obtain an a priori estimate for the pressure, a new splitting of the solution will be used. Let be $p_h^{m+1} = \overline{p}_h^{m+1} + \overline{\overline{p}}_h^{m+1}$, where the first part $\overline{p}_h^{m+1}$ is the solution of the problem

$$\frac{\kappa}{\eta}B\overline{p}_h^{m+1} = f_h^{m+1}, \quad m = 0, \ldots, M-1, \tag{22}$$

and the second $\overline{\overline{p}}_h^{m+1}$ is solution of

$$A\mathbf{u}_h^{m+1} + G\overline{\overline{p}}_h^{m+1} = \mathbf{g}_h^{m+1} - G\overline{p}_h^{m+1}, \tag{23}$$

$$\frac{D\mathbf{u}_h^{m+1} - D\mathbf{u}_h^m}{\tau} + \frac{\kappa}{\eta}B\overline{\overline{p}}_h^{m+1} + \frac{h^2B\left(\overline{\overline{p}}_h^{m+1} - \overline{\overline{p}}_h^m\right)}{4\tau(\lambda+2\mu)} = -\frac{h^2}{4(\lambda+2\mu)}B\frac{\overline{p}_h^{m+1}-\overline{p}_h^m}{\tau}. \tag{24}$$

We get from (23) and (24)

$$\tau \left\| \frac{\mathbf{u}_h^{m+1}-\mathbf{u}_h^m}{\tau} \right\|_A^2 + \left(G\left(\bar{\bar{p}}_h^{m+1}-\bar{\bar{p}}_h^m\right), \frac{\mathbf{u}_h^{m+1}-\mathbf{u}_h^m}{\tau} \right) = -\left(G\left(\bar{p}_h^{m+1}-\bar{p}_h^m\right), \frac{\mathbf{u}_h^{m+1}-\mathbf{u}_h^m}{\tau} \right) + \left(\mathbf{g}_h^{m+1}-\mathbf{g}_h^m, \frac{\mathbf{u}_h^{m+1}-\mathbf{u}_h^m}{\tau} \right)$$

and

$$\left(D\frac{\mathbf{u}_h^{m+1}-\mathbf{u}_h^m}{\tau}, \bar{\bar{p}}_h^{m+1}-\bar{\bar{p}}_h^m \right) + \frac{\kappa}{\eta}\left(B\bar{\bar{p}}_h^{m+1}, \bar{p}_h^{m+1}-\bar{\bar{p}}_h^m \right) + \frac{h^2}{4(\lambda+2\mu)}\left(B\frac{\bar{\bar{p}}_h^{m+1}-\bar{\bar{p}}_h^m}{\tau}, \bar{p}_h^{m+1}-\bar{\bar{p}}_h^m \right) = -\frac{h^2}{4(\lambda+2\mu)}\left(B\frac{\bar{p}_h^{m+1}-\bar{p}_h^m}{\tau}, \bar{\bar{p}}_h^{m+1}-\bar{\bar{p}}_h^m \right).$$

After adding these equations and simple transformations, we obtain the inequality

$$\frac{\kappa}{2\eta}\left(\|\bar{\bar{p}}_h^{m+1}\|_B^2 - \|\bar{\bar{p}}_h^m\|_B^2 \right) \le \frac{\tau}{2}\left\| G\left(\frac{\bar{p}_h^{m+1}-\bar{p}_h^m}{\tau}\right)\right\|_{A^{-1}}^2 + \frac{\tau h^2}{16(\lambda+2\mu)}\left\|\left(\frac{\bar{p}_h^{m+1}-\bar{p}_h^m}{\tau}\right)\right\|^2 + \frac{\tau}{2}\left\| \frac{\mathbf{g}_h^{m+1}-\mathbf{g}_h^m}{\tau}\right\|_{A^{-1}}^2$$

obtaining estimate (14). □

Convergence results are straightforward using estimates (13) and (14) and by considering the approximation errors of the scheme.

4 Multigrid solution method

Traditional understanding of multigrid is based on the insight that a smoothing method reduces high frequency components of an error between numerical approximation and the exact numerical solution, and a coarse grid correction based on standard grid coarsening handles the low frequency error components. It is the challenge to determine suitable multigrid components, like multigrid smoothers, for the discrete system under consideration. We search for an efficient multigrid solver for the perturbed poroelasticity equations discretized on collocated grids. With respect to the coarse grid correction, we choose geometric grid coarsening on the Cartesian grids, i.e. the sequence of coarse grids is obtained by doubling the mesh size in each spatial direction, and the multigrid transfer operators, from fine-to-coarse and from coarse-to-fine, can easily be adopted from scalar geometric multigrid. Suitable smoothing is the interesting issue here. Insights in smoothers for stabilized versions of the incompressible Navier–Stokes equations on collocated grids [9] can be used to set up efficient smoothers.

In detail, we will consider four different smoothers. Firstly, we construct a point-wise collective Gauss–Seidel relaxation, i.e., at each grid point, three unknowns $u_{i,j}, v_{i,j}$ and $p_{i,j}$ are solved simultaneously. This means that a small 3×3 system must be solved for each grid point. It is convenient to consider the correction equations,

$$\begin{pmatrix} a_{1,1} & a_{1,2} & a_{1,3} \\ a_{2,1} & a_{2,2} & a_{2,3} \\ a_{3,1} & a_{3,2} & a_{3,3} \end{pmatrix} \begin{pmatrix} \delta u_{i,j} \\ \delta v_{i,j} \\ \delta p_{i,j} \end{pmatrix}^{n+1} = \begin{pmatrix} r_{i,j}^1 \\ r_{i,j}^2 \\ r_{i,j}^3 \end{pmatrix}^n,$$

where $\delta \mathbf{u}_{i,j}^{n+1} = \mathbf{u}_{i,j}^{n+1} - \mathbf{u}_{i,j}^n$, $\delta p_{i,j} = p_{i,j}^{n+1} - p_{i,j}^n$ and $(r_{i,j}^l)^n$ represents the residual of equation $l (l = 1,2,3)$ of the system corresponding to node (i,j). The correction is added with a relaxation parameter ω: $\mathbf{u}_{i,j}^{n+1} = \mathbf{u}_{i,j}^n + \omega\delta\mathbf{u}_{i,j}^{n+1}$, $p_{i,j}^{n+1} = p_{i,j}^n + \omega\delta p_{i,j}^{n+1}$. As a second smoother, we include the alternating line Gauss–Seidel relaxation. This is a straightforward generalization of the point-wise collective smoother. For each line a block tridiagonal matrix has to be inverted.

The third coupled smoother, sometimes called box relaxation, updates all unknowns appearing in the discrete divergence operator in Eq. (7) simultaneously. In practice, this means that five unknowns $(p_{i,j}, u_{i+1,j}, u_{i-1,j}, v_{i,j+1}, v_{i,j-1})$ centered around a pressure point are relaxed simultaneously. Therefore, for each box a small 5×5 matrix must be inverted using the respective four equilibrium equations and the mass conservation equation in the center of the box (see Fig. 1).

Finally, we also evaluate the line-version of box smoothing, an alternating box-line Gauss–Seidel. For example, in the case of box x-line relaxation, this means

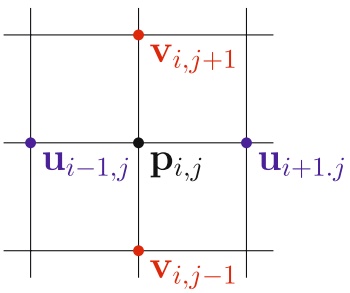

Fig. 1 Five unknowns centered around a pressure point updated simultaneously

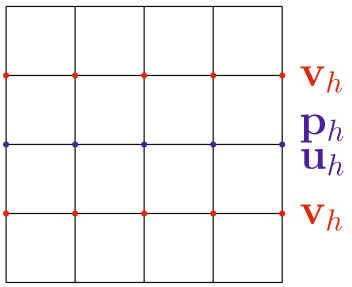

Fig. 2 Unknowns updated simultaneously by box x-line relaxation

that all unknowns marked in Fig. 2 are updated collectively.

5 Numerical experiments

5.1 Analytic solution of 2D model problem

We start this section by solving numerically a poroelasticity problem with a simple analytic solution given by

$$u = \cos(\pi x)\sin(\pi y)\sin(\pi t),$$
$$v = \sin(\pi x)\cos(\pi y)\sin(\pi t),$$
$$p = -2(\lambda + 2\mu)\pi \sin(\pi x)\sin(\pi y)\sin(\pi t).$$

Source term f is consequently determined. Due to the smooth solution in this problem we do not expect unphysical oscillations. However, with this example we show that the stabilization term, $h^2\Delta p_t/4(\lambda+2\mu)$, does not introduce too much artificial diffusion. In the example in Sect. 5.2, we will see that the stabilization term eliminates unphysical oscillations in the solution of the pressure completely. Tables 1 and 2 present the difference between analytic and numerical solution in the maximum norm at final time $t = 0.5$ for the reference parameter set $\lambda = 8333, \mu = 12500, k = 10^{-3}$ without and with the artificial pressure term, respectively. As for this example Crank–Nicolson scheme has been adopted, we also see in Table 2 that second order accuracy is maintained. On the other hand, if we omit $4(\lambda+2\mu)$ in the artificial term, i.e. if we consider an artificial term like

Table 1 Maximum norm of the error for displacements and for pressure with unperturbed collocated scheme (not stable)

Grid	$\frac{\|\|u_h-u\|\|_\infty}{\|\|u\|\|_\infty}$	$\frac{\|\|p_h-p\|\|_\infty}{\|\|p\|\|_\infty}$
$16\times16\times2$	0.00214	0.003965
$32\times32\times4$	0.000534	0.000983
$64\times64\times8$	0.000132	0.0002425
$128\times128\times16$	3.2873×10^{-5}	5.89612×10^{-5}

Table 2 Maximum norm of the error for displacements and for pressure with the term $h^2\Delta p_t/4(\lambda+2\mu)$ in the equations

Grid	$\frac{\|\|u_h-u\|\|_\infty}{\|\|u\|\|_\infty}$	$\frac{\|\|p_h-p\|\|_\infty}{\|\|p\|\|_\infty}$
$16\times16\times2$	0.00216	0.004074
$32\times32\times4$	0.0005389	0.001008
$64\times64\times8$	0.000133	0.0002474
$128\times128\times16$	3.2958×10^{-5}	5.9487×10^{-5}

Table 3 Maximum norm of the error for displacements and for pressure adding the term $h^2\Delta p_t$

Grid	$\frac{\|\|u_h-u\|\|_\infty}{\|\|u\|\|_\infty}$	$\frac{\|\|p_h-p\|\|_\infty}{\|\|p\|\|_\infty}$
$16\times16\times2$	0.3010	0.9101
$32\times32\times4$	0.2449	0.7286
$64\times64\times8$	0.10232	0.3048
$128\times128\times16$	0.01182	0.0351

$h^2\Delta p_t$ we introduce too much diffusion obtaining incorrect results as can be seen in Table 3. Details about the multigrid convergence are given in the discussion of the next problem.

5.2 Poroelastic footing experiment

The second example is a true 2D footing problem, see also [10]. The simulation domain is a 100 by 100 m block of porous soil, $\Omega = (-50, 50)\times(0, 100)$, as in Fig. 3.

At the base of this domain the soil is assumed to be fixed while at some centered upper part of the domain a uniform load of intensity σ_0 is applied in a strip of length 40 m. The whole domain is assumed free to drain. More

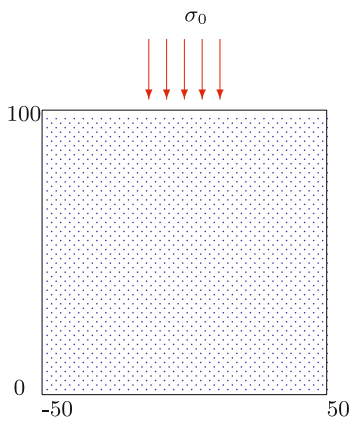

Fig. 3 Computational domain for the footing problem

Table 4 Material parameters for the second poroelastic problem

Property	Value	Unit
Young's modulus	3×10^4	N/m^2
Poisson's ratio	0.2	–
Permeability	10^{-7}	m^2
Fluid viscosity	10^{-3}	Pas

precisely, the boundary data are given as follows:

$$\begin{aligned} p &= 0, && \text{on } \partial\Omega, \\ \sigma_{xy} = 0, \sigma_{yy} &= -\sigma_0, && \text{on } \Gamma_1, \\ \sigma_{xy} = 0, \sigma_{yy} &= 0, && \text{on } \Gamma_2, \\ \mathbf{u} &= \mathbf{0}, && \text{on } \partial\Omega \setminus (\Gamma_1 \cup \Gamma_2), \end{aligned}$$

where $\sigma_{xy} = \mu\left(\frac{\partial u}{\partial y} + \frac{\partial v}{\partial x}\right)$, $\sigma_{yy} = \lambda\frac{\partial u}{\partial x} + (\lambda + 2\mu)\frac{\partial v}{\partial y}$, and

$$\Gamma_1 = \{(x, y) \in \partial\Omega, / \ |x| \le 20, y = 100\},$$
$$\Gamma_2 = \{(x, y) \in \partial\Omega, / \ |x| > 20, y = 100\}.$$

The material properties of the porous medium are given in Table 4 where λ and μ are related to Young's modulus E and Poisson's ratio ν by

$$\lambda = \frac{\nu E}{(1+\nu)(1-2\nu)}, \quad \mu = \frac{E}{2(1+\nu)}.$$

The uniform load is taken as $\sigma_0 = 10^4\,N/m^2$.

Notice that the boundary condition for the footing problem involves the prescription of stress conditions. A second order discretization of these boundary conditions is explained below. We consider, for example, a node (x, y) at Γ_1, where the boundary conditions read

$$\mu\left(\frac{\partial u}{\partial y} + \frac{\partial v}{\partial x}\right) = 0, \tag{25}$$

$$\lambda\frac{\partial u}{\partial x} + (\lambda + 2\mu)\frac{\partial v}{\partial y} = \sigma_0. \tag{26}$$

With the use of the poroelasticity equation

$$-(\lambda + 2\mu)\frac{\partial^2 u}{\partial x^2} - \mu\frac{\partial^2 u}{\partial y^2} - (\lambda + \mu)\frac{\partial^2 v}{\partial x \partial y} + \frac{\partial p}{\partial x} = 0,$$

we find

$$\begin{aligned} u(x, y - h) &= u(x, y) - h\frac{\partial u}{\partial y}(x, y) \\ &- \frac{h^2}{2\mu}\left((\lambda + 2\mu)\frac{\partial^2 u}{\partial x^2}(x, y) + (\lambda + \mu)\frac{\partial^2 v}{\partial x \partial y}(x, y)\right. \\ &\left. - \frac{\partial p}{\partial x}(x, y)\right) + O(h^3). \end{aligned}$$

So, in order to approximate boundary condition (25), we consider the second order difference approximation

$$\frac{2\mu}{h}\left(u_{\bar{y}} + v_{\overset{\circ}{x}}\right) - (\lambda + 2\mu)u_{\bar{x}x} - (\lambda + \mu)v_{x\bar{y}} = 0.$$

Similarly, to approximate boundary condition (26) we can employ the second order approximation

$$\frac{2}{h}\left((\lambda + 2\mu)v_{\bar{y}} + \lambda u_{\overset{\circ}{x}}\right) - \mu v_{\bar{x}x} - (\lambda + \mu)u_{x\bar{y}} + p_{\bar{y}} = \frac{2\sigma_0}{h}.$$

Figures 4 and 5 show that standard central finite differences for the original system of equations on a 40^2-grid lead to spurious oscillations in the discrete pressure at time $t = 0.01$. These unphysical oscillations do not occur with the stabilization term $h^2\Delta p_t/4(\lambda+2\mu)$ added to the equation, as seen in Figs. 6 and 7. On the other hand, as also shown in Sect. 5.1, if $4(\lambda + 2\mu)$ is omitted in the artificial term too much diffusion is introduced, yielding incorrect results (seen in Figs. 8 and 9).

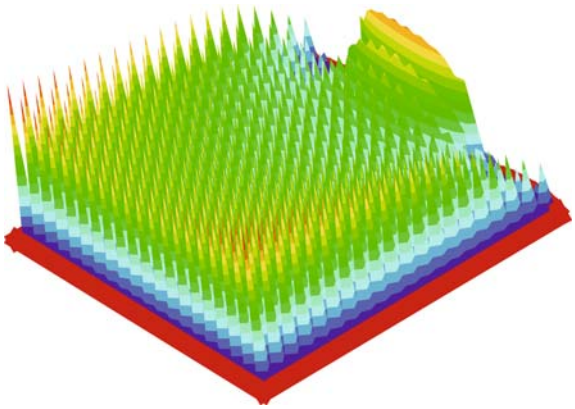

Fig. 4 Numerical solution for pressure for 2D poroelasticity reference problem, 40^2-grid without stabilization term

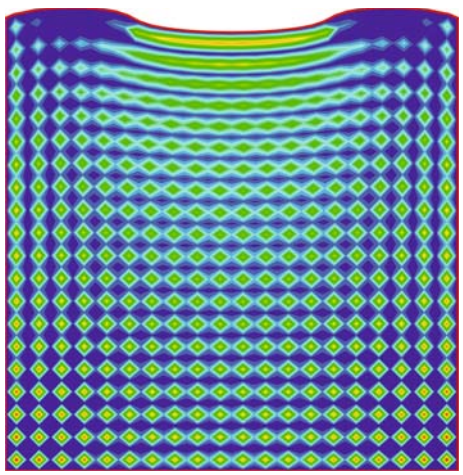

Fig. 5 Numerical solution for pressure for 2D poroelasticity reference problem, 40^2-grid without stabilization term

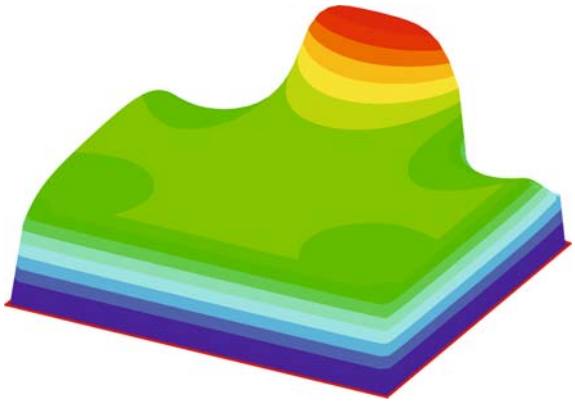

Fig. 6 Oscillation-free numerical solution for pressure for 2D poroelasticity reference problem, 40^2-grid adding the term $h^2\Delta p_t/4(\lambda+2\mu)$

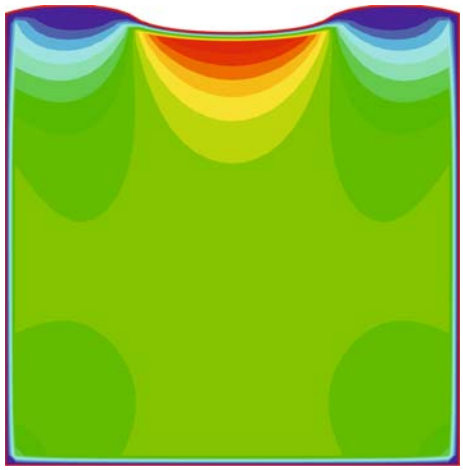

Fig. 7 Oscillation-free numerical solution for pressure for 2D poroelasticity reference problem, 40^2-grid adding the term $h^2\Delta p_t/4(\lambda+2\mu)$

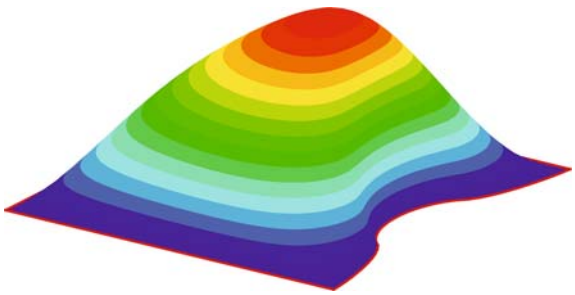

Fig. 8 Numerical solution for pressure for 2D poroelasticity reference problem with too much artificial diffusion, 40^2-grid adding the term $h^2\Delta p_t$

This problem is solved iteratively by multigrid with the smoothing methods proposed above. The stopping criterion per time step is that the absolute residual should be less than 10^{-6}. In Table 5 we show multigrid convergence results using the alternating box-line

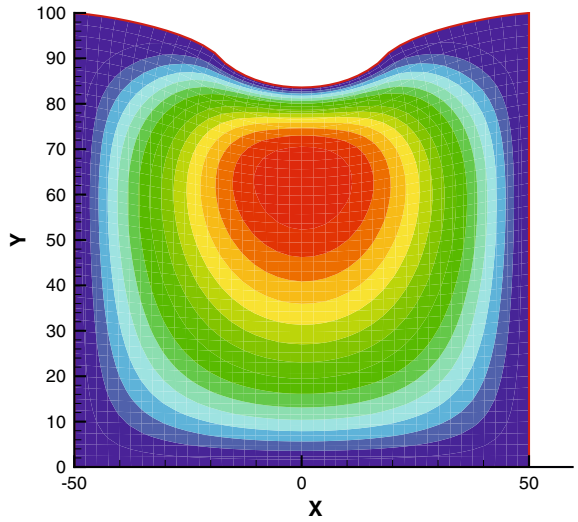

Fig. 9 Numerical solution for pressure for 2D poroelasticity reference problem with too much artificial diffusion, 40^2-grid adding the term $h^2\Delta p_t$

Table 5 F(1,0)-cycle, alternating box-line smoother, number of cycles and CPU time

Grid	Number of cycles	CPU time(s)
40×40	11	2
80×80	11	4
160×160	11	11
320×320	11	46

smoother from Sect. 4. The F(1,0)-cycle [12], meaning one pre-smoothing, no post-smoothing steps, is used each time step. The CPU time for this system on a Pentium IV, 2.6 GHz is 11 s on a 160^2-grid, and 46 s per time step on a 320^2-grid. A fast and h-independent behaviour is observed with on average 11 cycles per time step.

In the next experiments, based on the footing problem, we perform a systematic parameter study. In particular, we vary the quantity κ/η. For all tests in the following, F(2,1)-cycles are used.

Figure 10 presents the convergence for the alternating box-line smoother for different values of κ/η. For all values of κ/η very satisfactory convergence is obtained by the smoother. Figure 11 then shows the corresponding convergence with the point-wise box smoother. It can be observed that this smoother is sensitive to the size of the diffusion coefficient. For small values the method does not longer converge. For large values, however, the convergence is very satisfactory. Figure 12 presents the multigrid convergence for the alternating line Gauss–Seidel smoother. For small values of κ/η, like $\kappa/\eta = 10^{-4}$, the convergence is unsatisfactory. For completeness also the results with the point-wise Gauss–Seidel

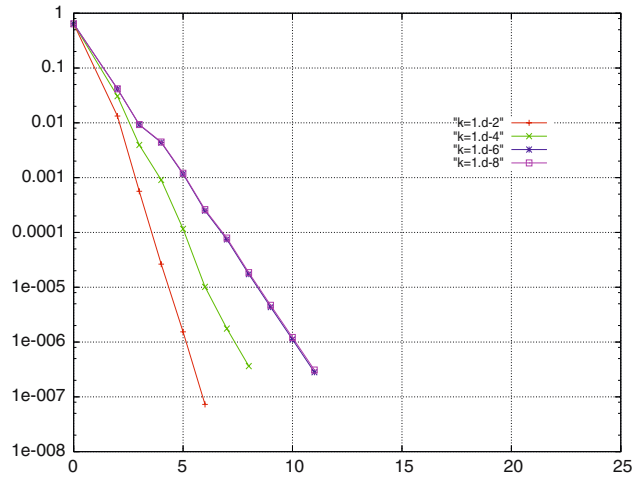

Fig. 10 F(2,1)-convergence with the alternating box-line smoother with a grid 320^2 for different values of k, $k/\eta = 10^{-2}, 10^{-4}, 10^{-6}, 10^{-8}$

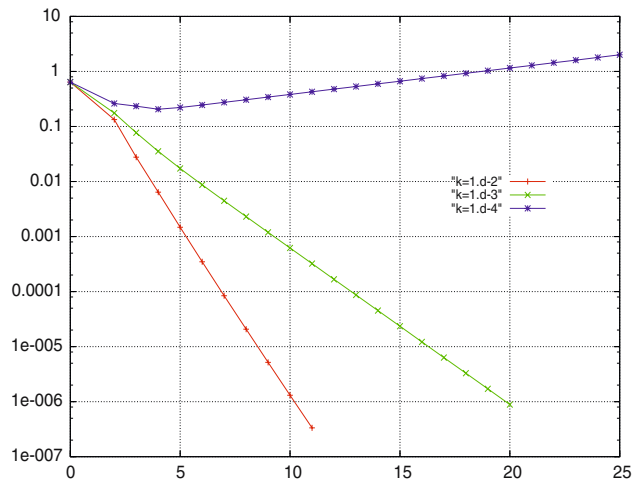

Fig. 11 F(2,1)-convergence with the box smoother with a grid 320^2 for different values of k/η, $k/\eta = 10^{-2}, 10^{-3}, 10^{-4}$

smoother are presented in Fig. 13. Obviously, for $\kappa/\eta = 10^{-4}$ the point-wise smoother also does not perform well. From this experiment, the box-line smoother is to be preferred, as it results in a robust convergence.

We evaluate this box-line smoother in more detail as we let ν tend to 0.5 in the experiments shown in Table 6. For satisfactorily convergence in this extreme parameter range, we have to choose overrelaxation parameter $\omega = 1.3$. In the table we observe for this value of ω a fast and robust multigrid convergence in the limit $\nu \to 0.5$. The choice of overrelaxation parameter is expected to be confirmed by local Fourier analysis. This is not done here.

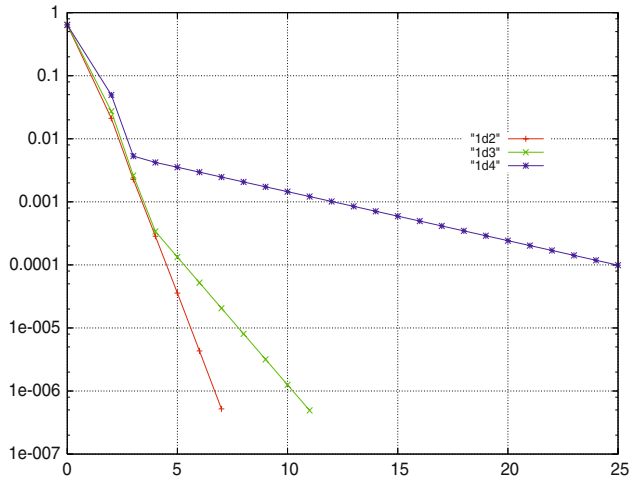

Fig. 12 F(2,1)-convergence with the line smoother with a grid 320^2 for different values of k, $k/\eta = 10^{-2}, 10^{-3}, 10^{-4}$

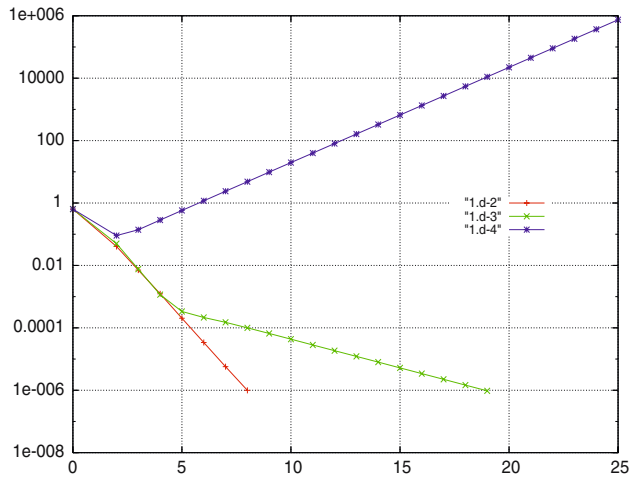

Fig. 13 F(2,1)-convergence with the point Gauss–Seidel smoother with a grid 320^2 for different values of k, $k/\eta = 10^{-2}$, $10^{-3}, 10^{-4}$

Table 6 F(2,1) multigrid convergence factors, and, in brackets, the average number of iterations per time step for different ν-values in the second poroelasticity test problem

	Grid			
	40×40	80×80	160×160	320×320
$\nu = 0.2$	0.30 (10)	0.35 (11)	0.23 (9)	0.2 (9)
$\nu = 0.3$	0.25 (9)	0.35 (12)	0.20 (9)	0.17 (8)
$\nu = 0.35$	0.21 (8)	0.38 (12)	0.20 (9)	0.13 (8)
$\nu = 0.4$	0.16 (7)	0.37 (12)	0.22 (9)	0.11 (7)
$\nu = 0.45$	0.26 (9)	0.30 (10)	0.22 (9)	0.22 (10)

6 Conclusions

In this paper we have presented an accurate and stable discretization for the 2D incompressible poroelasticity

equations on a collocated grid. Stabilization is done by adding an extra term in one of the continuous equations. It has been proved that a stable and accurate solution is obtained with this new set of poroelastic equations. Numerical experiments confirm the theory. In addition, an efficient multigrid method is constructed for consolidation type problems on Cartesian grids. This is done on the basis of box relaxation; its robust variant being the alternating box-line relaxation. We have also shown that box-line relaxation is robust for a wide range of values of the Lamé coefficients, if overrelaxation is employed. So, box relaxation is also of importance for multigrid efficiency on collocated grids. The other multigrid components are standard. The treatment of stress boundary conditions, as they appear for a poroelastic footing experiment do not pose substantial difficulties to the multigrid method.

References

1. Biot, M.: General theory of three dimensional consolidation. J. Appl. Phys. **12**, 155–169 (1941)
2. Biot, M.: Theory of elasticity and consolidation for a porous anisotropic solid. J. Appl. Phys. **33**, 182–185 (1955)
3. Biot, M.: General solutions of the equation of elasticity and consolidation for a porous material. J. Appl. Mech. **78**, 91–96 (1956)
4. Gaspar, F.J., Lisbona, F.J., Vabishchevich, P.N.: A finite difference analysis of Biot's consolidation model. Appl. Numer. Math. **44**, 487–506 (2003)
5. Gaspar, F.J., Lisbona, F.J., Vabishchevich, P.N.: Staggered grid discretizations for the quasi-static Biot's consolidation problem. Appl. Numer. Math. **56**, 888–898 (2006)
6. Gaspar, F.J., Lisbona, F.J., Oosterlee, C.W., Wienands, R.: A systematic comparison of coupled and distributive smoothing in multigrid for the poroelasticity system. Numer. Linear Algebra Appl. **11**, 93–113 (2004)
7. Gaspar, F.J., Lisbona, F.J., Oosterlee, C.W., Vabishchevich, P.N.: An efficient multigrid solver for a reformulated version of the poroelasticity system. Comput. Methods Appl. Mech. Eng. **196**, 1447–1457 (2007)
8. Korsawe, J., Starke, G.: A least-squares mixed finite element method for Biot's consolidation problem in porous media. SIAM J. Numer. Anal. **43**, 318–339 (2005)
9. Linden, J., Steckel, B., Stüben, K.: Parallel multigrid solution of the Navier–Stokes equations on general 2D-domains. Parallel Comput. **7**, 461–475 (1988)
10. Murad, M.A., Loula, A.F.D.: On stability and convergence of finite element approximations of Biot's consolidation problem. Int. J. Numer. Methods Eng. **37**, 645–667 (1994)
11. Samarskii, A.A.: Theory of Difference Schemes. Marcel Dekker, New York (2001)
12. Trottenberg, U., Oosterlee, C.W., Schüller, A.: Multigrid. Academic Press, New York (2001)
13. Wienands, R., Gaspar, F.J., Lisbona, F.J., Oosterlee, C.W.: An efficient multigrid solver based on distributive smoothing for poroelasticity equations. Computing **73**, 99–119 (2004)